ACS APPLIED MATERIALS & INTERFACES

Research Article

www.acsami.org

Highly Crystalline Low Band Gap Polymer Based on Thieno[3,4-*c*]pyrrole-4,6-dione for High-Performance Polymer Solar Cells with a >400 nm Thick Active Layer

Jae Woong Jung,[†,§] Thomas P. Russell,[‡] and Won Ho Jo*[,†]

[†]Department of Materials Science and Engineering, Seoul National University, 1 Gwanak-ro, Gwanak-gu, Seoul 151-744, Korea

[‡]Department of Polymer Science and Engineering, University of Massachusetts, Amherst, Massachusetts 01003, United States

Supporting Information

ABSTRACT: Two thieno[3,4-*c*]pyrrole-4,6-dione (TPD)-based copolymers combined with 2,2′-bithiophene (BT) or (*E*)-2-(2-(thiophen-2-yl)vinyl)thiophene (TV) have been designed and synthesized to investigate the effect of the introduction of a vinylene group in the polymer backbone on the optical, electrochemical, and photovoltaic properties of the polymers. Although both polymers have shown similar optical band gaps and frontier energy levels, regardless of the introduction of vinylene bridge, the introduction of a π-extended vinylene group in the polymer backbone substantially enhances the charge transport characteristics of the resulting polymer due to its strong tendency to self-assemble and thus to enhance the crystallinity. An analysis on charge recombination in the active layer of a solar cell device indicates that the outstanding charge transport (μ = 1.90 $cm^2 \cdot V^{-1} \cdot s^{-1}$) of PTVTPD with a vinylene group effectively suppresses the bimolecular recombination, leading to a high power conversion efficiency (PCE) up to 7.16%, which is 20% higher than that (5.98%) of the counterpart polymer without a vinylene group (PBTTPD). More importantly, PTVTPD-based devices do not show a large variation of photovoltaic performance with the active layer thickness; that is, the PCE remains at 6% as the active layer thickness increases up to 450 nm, demonstrating that the PTVTPD-based solar cell is very compatible with industrial processing.

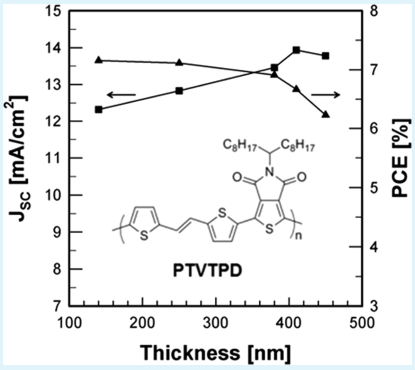

KEYWORDS: *polymer solar cell, thienylenevinylene, thick active layer*

INTRODUCTION

Polymer solar cells (PSCs) based on a bulk heterojunction (BHJ) structure that consists of a conjugated polymer and a fullerene derivative as an electron donor and acceptor, respectively, have emerged as a next-generation energy resource due to their unique advantages of low cost and large-area production by solution processing.[1−4] Over the past decade, alternating conjugated copolymers composed of electron-donating (D) and electron-accepting (A) units have been considered as the most promising donor material for high-performance PSCs because their frontier energy levels can effectively be tuned by proper combination of D and A units.[5] Moreover, molecular properties of D−A-type copolymers, such as the dipole moment, planarity of the backbone, intermolecular interaction, and charge transport characteristics, can also be fine-tuned by modifying each of the D and A units.[6−8] Specifically, the molecular design of the D−A structure for a conjugated polymer is the most effective strategy toward harvesting more photons by lowering the optical band gap, while the molecular energy levels satisfy the conditions for charge separation and transport.[9,10] In recent years, several D−A-type polymers have demonstrated promising photovoltaic performances close to 10% power conversion efficiency (PCE), demonstrating their high potential for commercialization of PSCs.[11−13]

Although most high-performance PSCs have achieved their best performance at a relatively thin active layer (ca. 100 nm), it is very difficult to fabricate reproducibly such thin films without a pinhole under current industrial processes. When the thickness of active layer is thicker, the bimolecular recombination of photoinduced charge carriers increases, and therefore, the resulting space charge decreases the fill factor (FF) due to the intrinsic low charge carrier mobility of organic semiconductors.[14,15] Therefore, one of the most challenging issues for mass production of PSCs is to fabricate thick active layers without large loss of photovoltaic performance.

Herein, we present highly crystalline D−A-type polymers based on thieno[3,4-*c*]pyrrole-4,6-dione (TPD). TPD possesses strong electron-withdrawing properties, leading to low frontier orbital energy levels of the corresponding conjugated polymers, which is beneficial to achieving a high open-circuit voltage (V_{OC}) of PSCs.[4,16−20] More importantly, highly fused and coplanar structure of TPD affords high crystallinity and

Received: April 24, 2015
Accepted: June 5, 2015
Published: June 5, 2015

DOI: 10.1021/acsami.5b03446
ACS Appl. Mater. Interfaces 2015, 7, 13666−13674

Scheme 1. Synthesis of the Polymers Studied in This Work

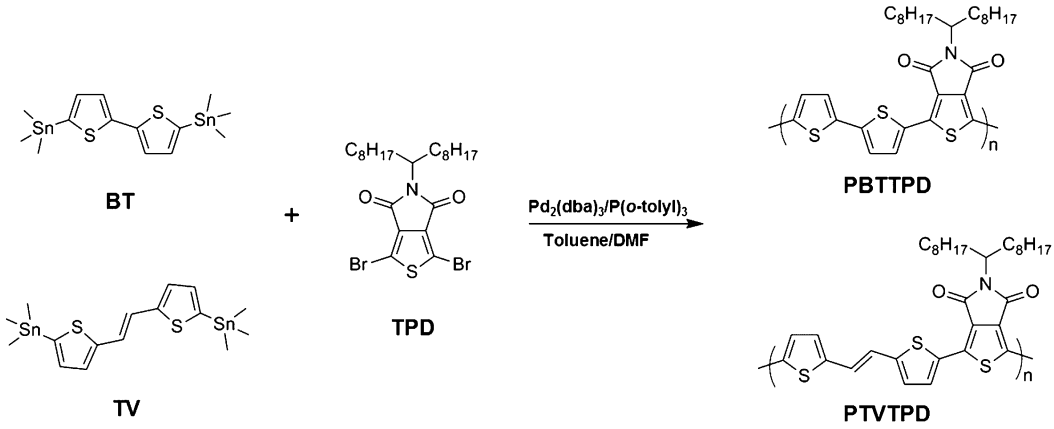

Table 1. Characteristics of the Polymers Synthesized in This Work

polymer	M_n (kDa)	PDI	$\lambda_{max,s}$ (nm)	$\lambda_{onset,s}$ (nm)	$\lambda_{max,f}$ (nm)	$\lambda_{onset,f}$ (nm)	LUMO[a] (eV)	HOMO[a] (eV)	E_g[a] (eV)	μ_h ($cm^2/V{\cdot}s$)
PBTTPD	44.7	1.73	532	695	579	700	−3.36	−5.511	2.15	0.56
PTVTPD	41.0	1.41	584	695	585	700	−3.32	−5.48	2.16	1.90

[a]Determined from cyclic voltammetry.

thus effective charge transport to the corresponding polymer, which are prerequisites for suppressing bimolecular recombination of charge carriers in BHJ films.[21,22] In conjunction with TPD, we adopted 2,2′-bithiophene (BT) and (*E*)-1,2-di-(thiophen-2-yl)ethane (simply called thienylenevinylene (TV)) as the D unit for constructing D−A-type polymers, PBTTPD and PTVTPD, respectively. TV has recently been recognized as a promising electron-donating unit of low band gap conjugated polymers for PSC application because the incorporation of a vinylene bridge in the polymer backbone enhances the planarity of the polymer backbone and thus affords strong $\pi-\pi$ interaction with a large overlapping area between chain backbones, leading to increased crystallinity of the conjugated polymer.[23−27] Hence, the PTVTPD with a π-extended TV unit shows significantly increased crystallinity and 3-fold larger hole mobility (1.90 $cm^2/V{\cdot}s$) than PTBTTPD without a vinylene unit (0.56 $cm^2/V{\cdot}s$), although the two copolymers exhibit similar optical band gaps and frontier energy levels. Furthermore, the high crystallinity of PTVTPD affords superior photoinduced charge generation with suppressed bimolecular recombination, which is beneficial for achieving high short-circuit current density (J_{SC}). Consequently, PTVTPD exhibits a high PCE exceeding 7% at a 140 nm thick active layer. It should be noted here that, during the preparation of our article, a polymer with the same polymer backbone as our PTVTPD but with a different alkyl side group on TPD was reported for photovoltaic applications.[28] They reported low hole mobility (1.72×10^{-2} $cm^2/V{\cdot}s$) and unsatisfactory PCE (4.68%) probably because of low molecular weight (~24 kDa) and low crystallinity, which are probably due to very long and branched side chains (5-decylheptadecane). However, PTVTPD with relatively short side chains (heptadecane) in our study has higher molecular weight (~41 kDa) and high crystallinity and thus exhibits much improved hole mobility (1.90 $cm^2/V{\cdot}s$) and higher PCE over 7%. More importantly, PTVTPD retains high photovoltaic performance over 6% PCE, while the active layer thickness increases from 140 to 450 nm, suggesting that the PTVTPD is a promising candidate as donor material for industrial production of PSCs.

RESULTS AND DISCUSSION

The synthetic routes of PBTTPD and PTVTPD are shown in Scheme 1. The polymers were synthesized by the Stille coupling reaction using $Pd_2(dba)_3$ and P(*o*-tol)$_3$ as catalyst and ligand, respectively. When the number-average molecular weights (M_n) and the polydispersity indexes (PDI) of the polymers were measured by gel permeation chromatography (GPC), all polymers had sufficient molecular weights (M_n > 40 kDa) with narrow PDIs for their device applications (Table 1).

When the optical properties of two polymers in solution as measured by UV−vis absorption spectroscopy are compared, it reveals that an identical absorption onset is observed at 695 nm for both polymers, corresponding to an optical band gap of 1.78 eV, while the maximum absorption peak (λ_{max} = 584 nm) of PTVTPD is red-shifted compared to PBTTPD (λ_{max} = 532 nm) (Figure 1 and Table 1). PTVTPD exhibits an obvious and intense vibronic shoulder peak at 640 nm in dilute solution at room temperature, indicating that the polymer chains are aggregated in solution. This is further evidenced by the disappearance of the shoulder peak at high solution temperature (Supporting Information Figure S1). Accordingly, for measurement of exact molecular weights of the polymers, the molecular weights of the polymers were measured at high temperature (120 °C) using a high-temperature GPC. A strong vibronic shoulder is also observed in solid film of PTVTPD, indicating that the PTVTPD exhibits strong interaction between polymer chains that may arise from increased conjugation length caused by a π-extended vinylene unit. It is noteworthy that the absorptivity of PTVTPD is higher than that of PBTTPD in both solution and the film state, which may arise from not only the extended π-conjugation by introduction of a vinylene bridge but also its better molecular stacking, as will be discussed in the following section.

To gain deeper insight into the effect of the vinylene moiety on the molecular structure and electronic property of the polymer, a theoretical calculation based on the density

DOI: 10.1021/acsami.5b03446
ACS Appl. Mater. Interfaces 2015, 7, 13666−13674

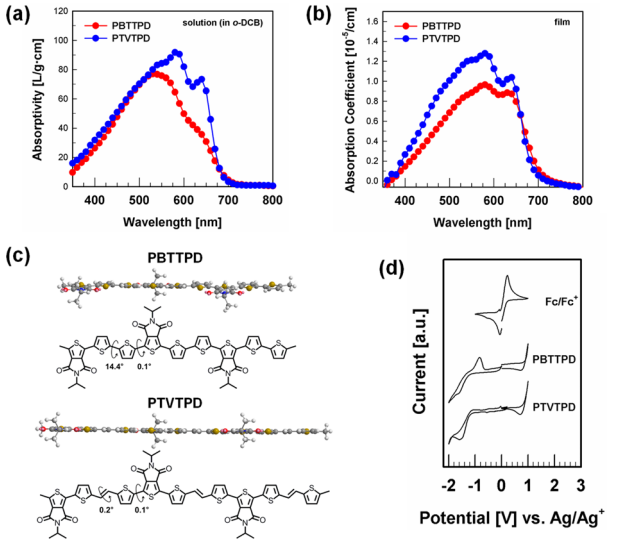

Figure 1. UV−vis absorption spectra (a) in solution and (b) in the thin film of the polymers. (c) Side view of repeating units of the polymers at the optimized geometries and (d) cyclic voltammograms of the polymers.

functional theory (DFT) at the B3LYP/6-31G* level was performed on the repeating unit of each polymer. As shown in Figure 1c, both polymers are expected to exhibit excellent planarity through the entire polymer backbone with small torsional angles at the optimized geometry. Although both polymers possess small dihedral angles close to 0° between TPD and thiophene, there is steric hindrance between adjacent thiophenes in PBTTPD (dihedral angle = 14.4°), while PTVTPD exhibits a very small torsional angle (<0.5°) between vinylene and the adjacent thiophene, indicating that the introduction of a vinylene bridge effectively reduces the steric hindrance between two thiophene units, allowing better planar conformation of the polymer backbone.

The effect of the vinylene unit on the electrochemical properties of the polymer was investigated by measuring the frontier energy levels (Figure 1d and Table 1). The highest occupied molecular orbital (HOMO) energy levels of PBTTPD and PTVTPD are −5.51 and −5.48 eV, respectively. These relatively low-lying HOMO levels may have a benefit to obtain high V_{OC} in PSCs because V_{OC} is proportional to the difference between the HOMO of the polymer donor and the lowest unoccupied molecular orbital (LUMO) of the PCBM acceptor. The LUMO levels of PBTTPD and PTVTPD were −3.36 and −3.32 eV, respectively. Therefore, it is realized that the introduction of a vinylene bridge does not significantly affect the frontier orbital energy levels of the resulting polymer, which is consistent with our previous report,[29] although PTVTPD exhibits energy levels slightly higher than those of PBTTPD due to the electron-rich nature of vinylene.

The crystallinity and molecular orientation of the polymers in the solid film state were examined by the grazing incidence wide-angle X-ray scattering (GIWAXS). As illustrated in Figure 2 and Supporting Information Figure S3, PBTTPD shows two distinct diffraction peaks at q_z = 0.29 and 0.59 Å^{-1}, while PTVTPD exhibits stronger peaks at q_z = 0.29, 0.59, 0.90, and 1.20 Å^{-1} in the out-of-plane (q_z) direction, corresponding to the typical (h00) diffraction of a well-ordered lamellar structure

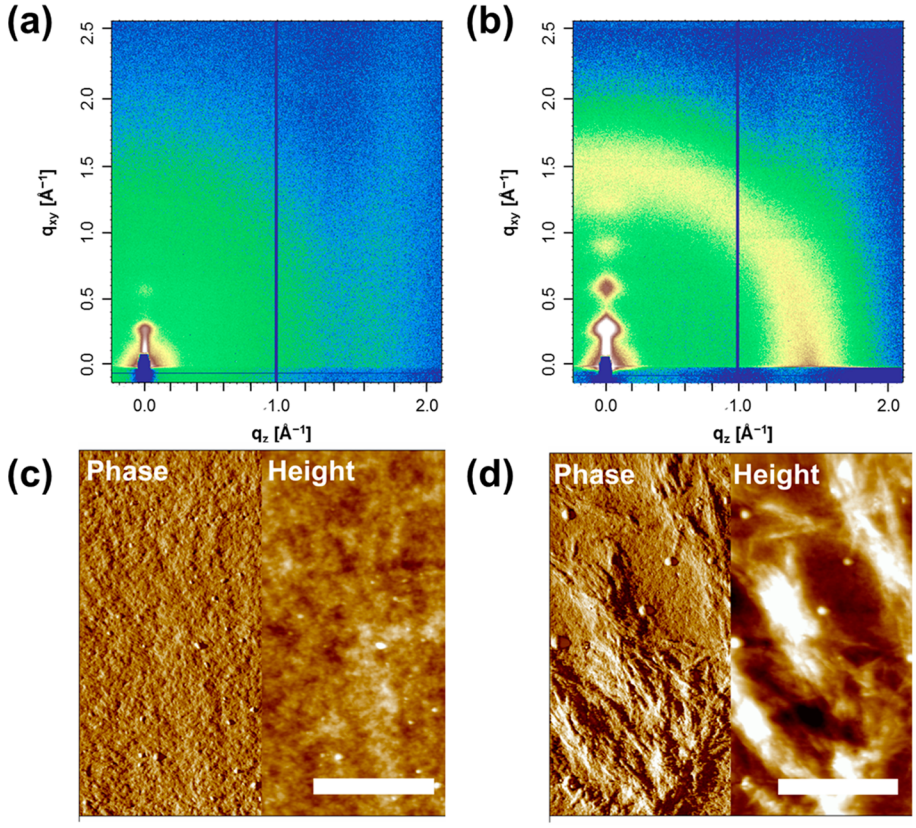

Figure 2. Two-dimensional GIWAXS images of (a) PBTTPD and (b) PTVTPD thin films. AFM images of (c) PBTTPD and (d) PTVTPD (scale bar is 1 μm).

DOI: 10.1021/acsami.5b03446
ACS Appl. Mater. Interfaces 2015, 7, 13666−13674

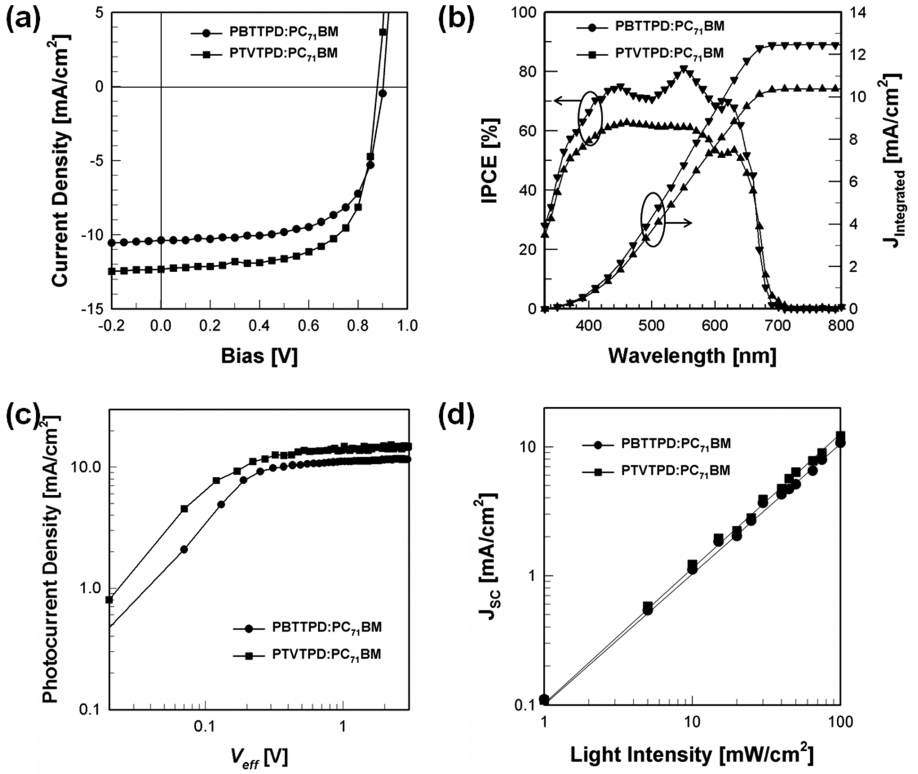

Figure 3. (a) J–V curves, (b) IPCE spectra (with integrated current densities), (c) plot of J_{ph} vs V_{eff}, and (d) plot of J_{SC} vs light intensity of PSC devices.

Table 2. Optimized Photovoltaic Properties of PSCs

active layer	V_{OC} (V)	J_{SC} (mA/cm^2)	$J_{SC/Cal.}$[c] (mA/cm^2)	FF	PCE[d] (%)	G_{max} (m^{-3}·s^{-3})	α
PBTTPD:PC$_{71}$BM[a]	0.90	10.38	10.31	0.64	5.98 (5.75)	3.76 × 1027	0.92
PTVTPD:PC$_{71}$BM[b]	0.88	12.32	12.47	0.66	7.16 (6.97)	8.13 × 1027	0.96

[a]Thickness = 140 nm. [b]Thickness = 110 nm. [c]Calculated J_{SC} obtained from the IPCE spectra of the best device. [d]Average PCE in parentheses (over 12 devices).

in an edge-on orientation with d_{100} = 21.7 Å.[30,31] Stronger diffraction of the PTVTPD film indicates that the incorporation of vinylene in the polymer backbone effectively enhances crystallization of PTVTPD. Another feature to be noted from GIWAXS is that PTVTPD exhibits an obvious (010) diffraction at q_z = 1.55 Å^{-1} that corresponds to the π–π stacking distance of 4.05 Å, while PBTTPD does not show a discernible (010) diffraction, demonstrating not only that PTVTPD has more closely packed structure in the π–π direction than PBTTPD but also that some crystallites of PTVTPD adopt the face-on orientation. Interestingly, the in-plane (q_{xy}) scan of GIWAXS for PTVTPD reveals an intense (100) peak at q_{xy} = 0.30 Å^{-1} that corresponds to an interchain distance of 20.9 Å (Supporting Information Figure S3), which is slightly shorter than the distance in the q_z direction (21.7 Å), indicating that polymer crystallites with face-on orientation are more densely packed than those with edge-on orientation. In short, the introduction of a vinylene unit enhances not only the crystallinity but also the face-on orientation of crystallites in the blend, which is very favorable for effective charge transport in photovoltaic devices.

The morphology of the polymer film is strongly dependent on the crystallinity of the polymer. As seen in Figure 2c,d, the PBTTPD film shows a smooth surface with a root mean square (rms) roughness of 3.37 nm, while the PTVTPD film exhibits a larger rms roughness of 9.81 nm, with a clearly fibrillar nanostructure. When the charge transport properties of the polymers are examined by measuring hole mobilities of PBTTPD and PTVTPD using field-effect transistors (FETs), both polymers exhibit the typical behavior of p-channel transport, as shown in Supporting Information Figure S2. PTVTPD showed a hole mobility (1.90 cm^2·V^{-1}·s^{-1}) higher than that of PBTTPD (0.56 cm^2·V^{-1}·s^{-1}) when the hole mobility was determined at the saturation regime using the relationship $\mu_{sat} = (2I_{DS}\cdot L)/(W\cdot C(V_G - V_{th})^2)$, where I_{DS} is the saturation drain current, C is capacitance (~11.5 nF·cm^{-2}) of the SiO_2 dielectric, V_G is gate bias, V_{th} is threshold voltage, W is channel width (1500 μm), and L is channel length (300 μm). This is because PTVTPD has a highly coplanar polymer backbone, which may afford a high degree of self-assembly of polymer chains and thus a crystallinity higher than that of PBTTPD, facilitating more efficient charge transport. Notably, 1.90 cm^2/V·s of PTVTPD is one of the highest hole mobilites for conjugated polymers.

For measurement of the photovoltaic performance of the polymers, BHJ solar cells with an inverted device architecture (ITO/ZnO/active layer/MoO_3/Ag) were fabricated using $PC_{71}BM$ as the electron acceptor. The optimal weight ratio of polymer to $PC_{71}BM$ was 1:4 for both polymers. Since the conventional device architecture exhibited inferior photovoltaic

DOI: 10.1021/acsami.5b03446
ACS Appl. Mater. Interfaces 2015, 7, 13666–13674

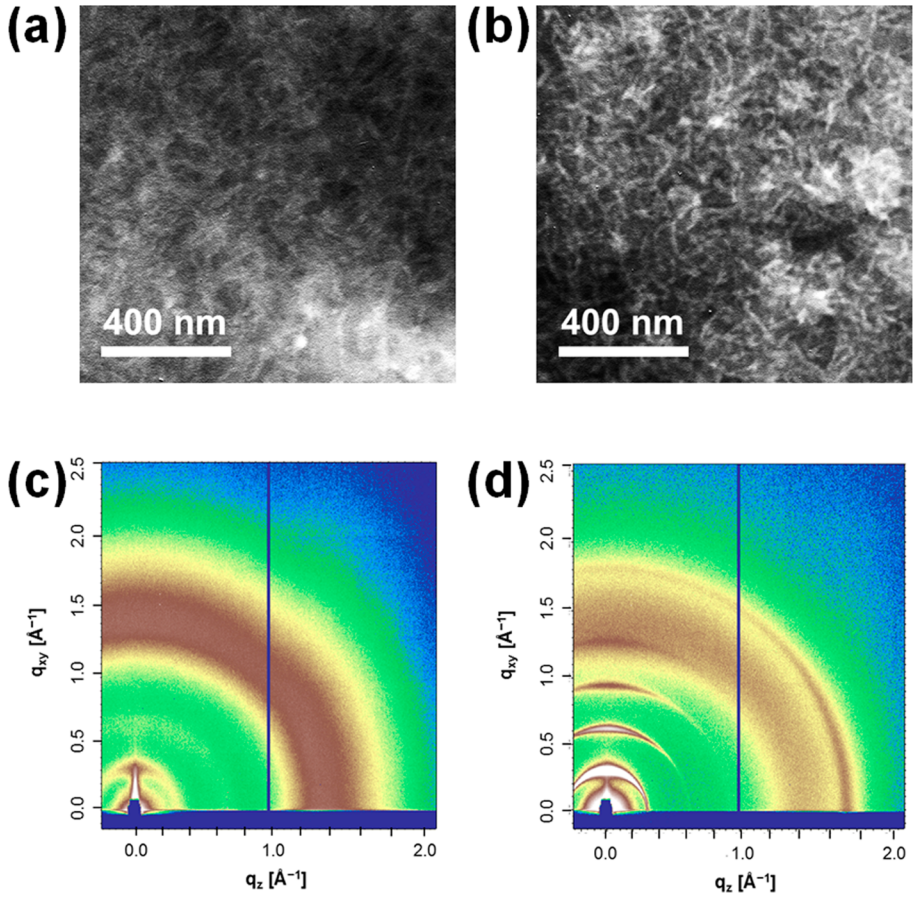

Figure 4. TEM images of (a) PBTTPD:$PC_{71}BM$ and (b) PTVTPD:$PC_{71}BM$ blends, and 2-D GIWAXS of (c) PBTTPD:$PC_{71}BM$ and (d) PTVTPD:$PC_{71}BM$ blends.

performance to the inverted one, all of the PSCs studied in this work were fabricated in the inverted device. Detailed data for the device optimization (the blend ratio, etc.) are listed in Supporting Information. When the active layer was spin-coated from *o*-dichlorobenzene (DCB) solution with 3 vol % of diiodooctane (DIO) as the processing additive, the best photovoltaic performance was obtained with a 140 nm thick film. The $J-V$ curves and the corresponding incident photon-to-current efficiency (IPCE) spectra of the PSC device under the optimized conditions are shown in Figure 3, and relevant photovoltaic parameters are listed in Table 2. The PBTTPD-based device shows a moderate PCE of 5.98% with a V_{OC} of 0.90 V, a J_{SC} of 10.38 mA/cm^2, and a FF of 0.64, while the PTVTPD-based one exhibits much improved performance of 7.16% PCE (V_{OC} of 0.88 V, J_{SC} of 12.32 mA/cm^2, and FF of 0.66). The IPCE spectra have shown that the PTVTPD-based device exhibits higher conversion efficiency in the range of 500−680 nm, which is consistent with the better light absorption of PTVTPD, as shown in Figure 1. The integrated current density calculated from IPCE spectra of both devices matches the J_{SC} values obtained from $J-V$ curves well (Table 2), indicating that the device performances of PSCs fabricated in this work are highly reliable. As expected from the low-lying HOMO energy levels of the polymers, both PSC devices exhibit relatively high V_{OC} values. The slightly higher V_{OC} of the PBTTPD-based device compared to that of the PTVTPD-based device is also consistent with the HOMO energy levels of the polymers. The PCE enhancement of the PTVTPD-based device arises mainly from increased J_{SC} and FF.

To further understand the enhancement of J_{SC}, the maximum exciton generation rates (G_{max}) of the devices are estimated by plotting the photocurrent density (J_{ph}) as a function of effective voltage (V_{eff}) ($J_{ph} = J_L - J_D$, where J_L and J_D are the current densities under illumination and dark conditions, respectively, and $V_{eff} = V_0 - V$, where V_0 is the voltage when $J_{ph} = 0$ and V is the applied bias). As can be seen in Figure 3c, J_{ph} was saturated as V_{eff} exceeds 1 V, and thus the value of G_{max} can be obtained from the equation of $J_{sat} = q \cdot L \cdot G_{max}$, where J_{sat} is the saturation photocurrent density, q is the electronic charge, and L is the thickness of the BHJ layer in the device.[32] The device based on the PTVTPD:$PC_{71}BM$ blend shows a G_{max} higher than that of PBTTPD:$PC_{71}BM$ (Table 2). Therefore, higher J_{SC} of PTVTPD may be ascribed to higher charge generation along with greater light absorptivity. When the ratio of J_{ph} to J_{sat} under short-circuit conditions was calculated to evaluate the overall exciton dissociation and charge collection efficiency, the ratios of PBTTPD- and PTVTPD-based devices were 0.88 and 0.94, respectively, indicating that the PTVTPD-based device exhibits a photoinduced charge generation higher than that of the PBTTPD-based one. Furthermore, the PTVTPD-based device shows higher J_{ph} in the entire V_{eff} range, indicating better photoinduced charge carrier generation and less recombination in the PTVTPD:$PC_{71}BM$ blend. The charge recombination kinetics of the solar cell device can be analyzed quantitatively by measuring J_{SC} as a function of light intensity (P_{light}) (Figure 3d). The relationship between J_{SC} and P_{light} can be represented by a power law equation: $J_{ph} \propto (P_{light})^{\alpha}$, where α is a recombination parameter.[33,34] Since $\alpha = 1$ corresponds to the

DOI: 10.1021/acsami.5b03446
ACS Appl. Mater. Interfaces 2015, 7, 13666−13674

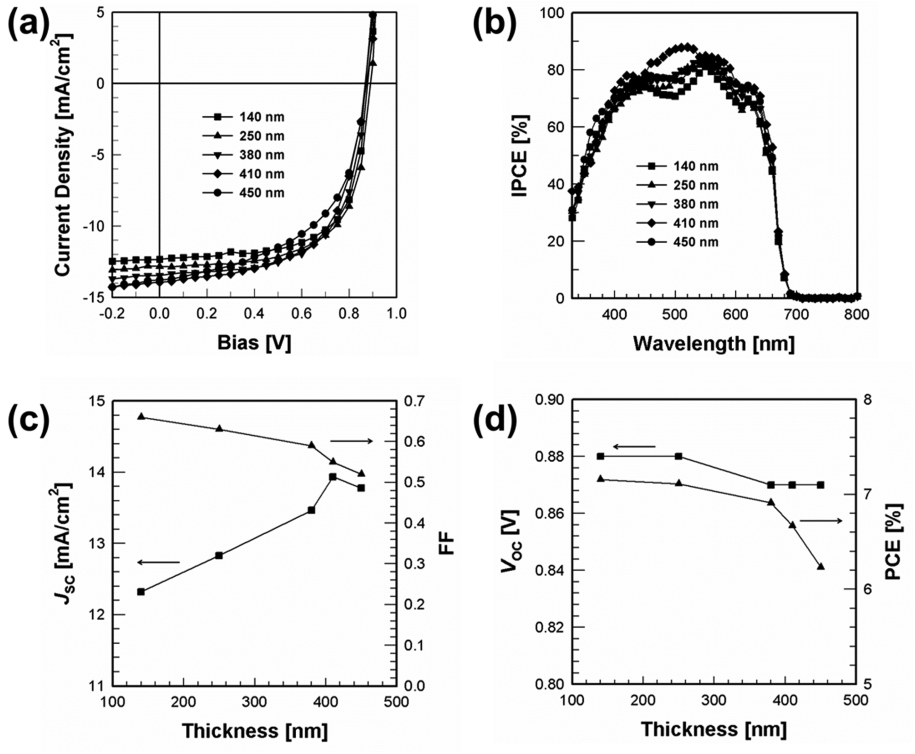

Figure 5. (a) $J-V$ curves, (b) IPCE spectra, and dependence of (c) J_{SC}/FF and (d) V_{OC}/PCE on the active layer thickness of PTVTPD-based solar cell devices.

absence of photocurrent loss due to bimolecular recombination, an α value for the PTVTPD-based device (0.96) higher than the value for the PBTTPD-based device (0.92) clearly indicates that bimolecular recombination is considerably suppressed in the PTVTPD:$PC_{71}BM$ blend. It is concluded from the above discussion that the improved light absorption, better photoinduced charge generation, efficient charge transport, and suppressed recombination in the PTVTPD-based device lead to superior photovoltaic performance.

The BHJ morphology of the PTVTPD:$PC_{71}BM$ blend as observed by transmission electron microscopy (TEM) shows a well-developed network structure of fibrils with a diameter of ca. 20 nm, which is comparable to the exciton diffusion length and thus favorable for exciton diffusion and dissociation, while the PBTTPD:$PC_{71}BM$ blend exhibits indistinct phase separation, as shown in Figure 4. Hence, it is expected that the PTVTPD-based device exhibits more effective charge generation than the PBTTPD-based one.

With better charge generation and transport of PTVTPD, we have also investigated the effect of active layer thickness on the device performance (Figure 5). As the thickness of the active layer increases, J_{SC} is expected to increase due to enhanced light absorption, while FF is generally decreased because of an increase of charge drift length in the thick active layer and thereby the increase of probability of charge recombination. As the active layer thickness of the PTVTPD:$PC_{71}BM$-based device was increased, J_{SC} increased continuously up to 410 nm and then saturated to the value of ca. 14 mA/cm^2 (Table 3). Contrary to general expectation, however, the decrease of FF with increasing active layer thickness was not so significant that it outweighs the gain of J_{SC} and thus decreases substantially the PCE (see Table 3 and Figure 5c), indicating that the charge recombination in thick films of PTVTPD: $PC_{71}BM$ is not so large, probably due to the high hole mobility of PTVTPD. As a consequence, the device with a 450 nm thick active layer retains a promising PCE of 6.3%. This insensitivity of photovoltaic performance to the active layer thickness provides PTVTPD with strong potential as a promising photovoltaic material compatible with industrial coating processes such as spray coating and roll-to-roll printing.

Table 3. Device Parameters of the PSCs Based on PTVTPD:$PC_{71}BM$ with Different Active Layer Thickness

thickness (nm)	V_{OC} (V)	J_{SC} (mA/cm^2)	$J_{SC,Cal.}$[a] (mA/cm^2)	FF	PCE[b] (%)
140	0.88	12.32	12.47	0.66	7.16 (6.97)
250	0.88	12.83	12.78	0.63	7.11 (6.83)
380	0.87	13.46	13.25	0.59	6.91 (6.41)
410	0.87	13.94	13.91	0.55	6.67 (6.35)
450	0.87	13.78	13.55	0.52	6.23 (6.03)

[a]Integrated J_{SC} from the IPCE spectra. [b]Average PCE in parentheses (over 12 devices).

The ambient stability is another critical issue for practical applications of PSCs. To quantitatively assess the ambient device stability, the devices were kept under ambient conditions (~30% relative humidity) in the dark for up to 80 h and subjected to $J-V$ measurement. As seen in Figure 6, the devices based PBTTPD and PTVTPD showed similar device stability. Specifically, the J_{SC} and FF decreased gradually upon exposure to ambient conditions, while V_{OC} retained 98% of the initial value after 80 h. As a result, both devices based on PBTTPD and PTVTPD retain 80% of the initial PCE after 80 h exposure in ambient atmosphere, demonstrating that the TPD-based devices exhibit promising device stability under ambient conditions.

DOI: 10.1021/acsami.5b03446
ACS Appl. Mater. Interfaces 2015, 7, 13666−13674

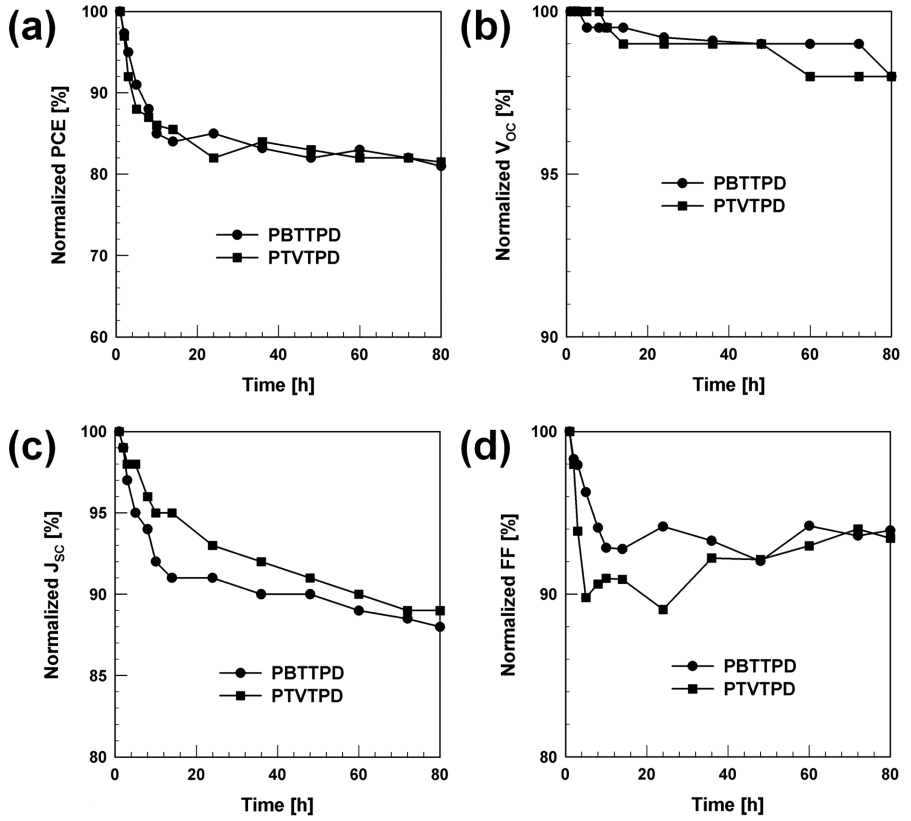

Figure 6. Variation of normalized PCE (a), V_{OC} (b), J_{SC} (c), and FF (d) of the solar cell devices based on PBTTPD and PTVTPD with ambient storage time.

CONCLUSION

We designed and synthesized TPD-based low band gap polymers for photovoltaic application. Incorporation of a vinylene group into the polymer backbone (PTVTPD) significantly improved the intermolecular interaction, resulting in increased light absorptivity, improved charge generation, and enhanced charge transport with reduced bimolecular recombination as compared to the polymer without the introduction of a vinylene bridge (PBTTPD). As a consequence, the PTVTPD-based PSC device exhibits 7.16% PCE, which is 20% higher than that of the PBTTPD-based device. Furthermore, the PTVTPD-based device retains a PCE greater than 6.3% without substantial loss of PCE as the active layer thickness increases up to 450 nm, demonstrating that PTVTPD is very compatible with industrial manufacturing processes for mass production of solar cells.

EXPERIMENTAL SECTION

Materials. All reagents were purchased from Sigma-Aldrich unless specified and used as received. 5,5′-Bis(trimethylstannyl)-2,2′-bithiophene (BT),[35] (*E*)-1,2-bis(5-(trimethylstannyl)thiophen-2-yl)-ethene (TV),[36] and 1,3-dibromo-5-(heptadecan-9-yl)-4*H*-thieno[3,4-*c*]pyrrole-4,6(5*H*)-dione (TPD)[37] were synthesized by following the methods reported in the literature. For the synthesis of PBTTPD, a solution of BT (98.4 mg, 0.2 mmol), TPD (109.9 mg, 0.2 mmol), and tri(*o*-tolyl)phosphine (9 mg, 0.03 mmol) was dissolved in 5 mL of an anhydrous toluene/DMF mixture (9/1 in volume), and the solution was degassed for 30 min. After the $Pd_2(dba)_3$ (5 mg, 0.005 mmol) was added to the solution, the mixture was refluxed for 48 h under nitrogen, followed by end-capping using 2-bromothiophene and 2-tributyltinthiophene successively. After being cooled to room temperature, the solution was precipitated in methanol, filtered, and then purified by Soxhlet extraction successively with methanol, acetone, hexane, methylene chloride, and chloroform. Finally, the chloroform fraction was concentrated and then precipitated in methanol. The dark purple solid was obtained in 64% yield after being filtered with a PTFE filter and dried overnight; M_n = 44.7 kDa, PDI = 1.73. ^{1}H NMR (300 MHz, $CDCl_3$, δ): 8.15−7.50 (br, 2H), 7.40−6.40 (br, 2H), 4.10−3.90 (br, 1H), 2.10−1.80 (br, 4H), 1.30 (m, 24H), 0.87 (m, 6H). Anal. Calcd for $C_{34}H_{45}NO_2S_3$: C, 68.53; H, 7.61; S, 16.14. Found: C, 68.64; H, 7.67; S, 16.02. For PTVTPD, 0.2 mmol of TV was used instead of BT, and the yield was 74%; M_n = 41.0 kDa, PDI = 1.41. ^{1}H NMR (300 MHz, $CDCl_3$, δ): 8.00−7.30 (br, 2H), 7.30−6.10 (br, 4H), 4.10−3.85 (br, 1H), 2.15−1.80 (br, 4H), 1.33 (m, 24H), 0.84 (m, 6H). Anal. Calcd for $C_{32}H_{43}NO_2S_3$: C, 67.44; H, 7.61; S, 16.88. Found: C, 67.55; H, 7.60; S, 16.92.

Characterization. Molecular weight and its distribution of polymers were measured by GPC (Polymer Laboratories GPC 220) with a refractive index detector at 120 °C using DCB as an eluent. The molecular weight of the polymer was calibrated by polystyrene standards. The optical absorption spectra were obtained by a UV−vis spectrophotometer (PerkinElmer Lamda 25). Cyclic voltammetry was conducted on a potentiostat/galvanostat (VMP3, Biologic) in an electrolyte solution of 0.1 M tetrabutylammonium hexafluorophosphate acetonitrile. Pt wires (Bioanalytical System Inc.) were used as both counter and working electrodes, and silver/silver ion (Ag in 0.1 M $AgNO_3$ solution, Bioanalytical System Inc.) was used as a reference electrode. The HOMO energy levels of polymers were calculated by using the equation HOMO (eV) = $[E_{ox} - E_{1/2(ferrocene)} + 4.8]$, where E_{ox} is the onset oxidation potential of the polymer and $E_{1/2(ferrocene)}$ is the onset oxidation potential of ferrocene vs Ag/Ag^+. DFT calculations at the B3LYP/6-31G(d,p) level were carried with Gaussian 09. Dipole moments in ground and excited states were calculated with time-dependent DFT. The charge transport characteristics of polymers were measured by thin film transistors (bottom-gate top-contact device geometry). On the heavily n-doped SiO_2/Si substrate, the spin-coated films (thickness of 50 nm) of polymers were coated from DCB

DOI: 10.1021/acsami.5b03446
ACS Appl. Mater. Interfaces 2015, 7, 13666−13674

solution. The surface of the substrate was treated with octadecyltrichlorosilane to afford a hydrophobic dielectric surface. Source and drain electrodes were then thermally evaporated (60 nm) with channel width (W) and length (L) of 1500 and 300 μm, respectively. All the devices were clearly isolated to achieve a negligible gate leakage current. The field-effect mobility was extracted from the saturation regime using the relationship $\mu_{sat} = (2 \cdot I_{DS} \cdot L)/[W \cdot C(V_G - V_{th})^2]$, where I_{DS} denotes the saturation drain current, C is the capacitance of the SiO_2 dielectric ($\sim$11.5 nF·cm^{-2}), V_G is the gate bias, and V_{th} is the threshold voltage. The device performance was evaluated in air using the 4200-SCS semiconductor characterization system.

Fabrication and Characterization of Polymer Solar Cells. Solar cell devices were fabricated with an inverted structure of ITO/ZnO (30 nm)/polymer:$PC_{71}BM$/MoO_3 (8 nm)/Ag (120 nm). The patterned indium tin oxide (ITO) glass was cleaned in an ultrasonic bath of acetone and isopropyl alcohol and treated in an ultraviolet–ozone chamber for 30 min. Then, the ZnO layer was fabricated via a sol–gel procedure from spin-coating of the ZnO precursor solution ($C_4H_6O_4Zn \cdot 2(H_2O)$ in 2-methoxyethanol and ethanolamine) onto the ITO-coated glass substrates.[38−40] After being thermally annealed at 200 °C for 1 h, the active layers were spin-coated from a polymer blend solution in DCB with 3 vol % of DIO. After being spin-coated, the films were placed in a closed jar to slowly dry the solvent. Finally, MoO_3 and Ag were thermally evaporated as an anode electrode at a pressure of less than 10^{-7} Torr. The active area of the device was 4.00 mm^2 as defined by a shadow mask that was fabricated by a laser beam technique. All masked tests gave consistent results within 1% error. The photovoltaic performance was measured under a nitrogen atmosphere inside a glovebox. The current density–voltage (J–V) curves were obtained with a Keithley 4200 source-meter under AM 1.5G (100 mW·cm^{-2}) illumination, which was accurately calibrated using a standard Si photodiode detector equipped with a KG-5 filter, which can be traced back to the standard cell of the National Renewable Energy Laboratory (NREL). The IPCE spectra of the devices were obtained from an IPCE setup consisting of a xenon lamp (Oriel, 450 W) as the light source, a monochromator, a chopper with a frequency of 100 Hz, a lock-in amplifier (SR830, Stanford Research Corp), and a Si-based diode (J115711-1-Si detector) for calibration. The calculated J_{SC} value was obtained by integrating the EQE spectrum under AM 1.5G illumination. For device stability analysis, the devices were stored in ambient conditions (dark, $\sim$30% relative humidity) and J–V curves were measured under AM 1.5G (100 mW·cm^{-2}) illumination by a Keithley 2400 source-meter in ambient conditions without any encapsulation.

■ ASSOCIATED CONTENT

Supporting Information

Additional data for UV–vis absorption, FET, GIWAXS, and solar cell devices. The Supporting Information is available free of charge on the ACS Publications website at DOI: 10.1021/acsami.5b03446.

■ AUTHOR INFORMATION

Corresponding Author

*E-mail: whjpoly@snu.ac.kr.

Present Address

[§](J.W.J.) Department of Materials Science and Engineering, University of Washington.

Notes

The authors declare no competing financial interest.

■ ACKNOWLEDGMENTS

The authors thank the Ministry of Education, Korea, for financial support through the Global Research Laboratory (GRL) program. T.P.R. also acknowledges the support of the U.S. Department of Energy through the Energy Frontier Research Center.

■ REFERENCES

(1) Thompson, B. C.; Fréchet, J. M. J. Polymer–Fullerene Composite Solar Cells. *Angew. Chem., Int. Ed.* **2008**, *47*, 58–77.

(2) Chochos, C. L.; Choulis, S. A. How the Structural Deviations on the Backbone of Conjugated Polymers Influence Their Optoelectronic Properties and Photovoltaic Performance. *Prog. Polym. Sci.* **2011**, *36*, 1326–1414.

(3) Jung, J. W.; Jo, J. W.; Jo, W. H. Enhanced Performance and Air Stability of Polymer Solar Cells by Formation of a Self-Assembled Buffer Layer from Fullerene-End-Capped Poly(ethylene glycol). *Adv. Mater.* **2011**, *23*, 1782–1787.

(4) Small, C. E.; Chen, S.; Subbiah, J.; Amb, C. M.; Tsang, S.-W.; Lai, T.-H.; Reynolds, J. R.; So, F. High-Efficiency Inverted Dithienogermole-Thienopyrrolodione-Based Polymer Solar Cells. *Nat. Photonics* **2012**, *6*, 115–120.

(5) You, J.; Dou, L.; Yoshimura, K.; Kato, T.; Ohya, K.; Moriarty, T.; Emery, K.; Chen, C.-C.; Gao, J.; Li, G.; Yang, Y. A Polymer Tandem Solar Cell with 10.6% Power Conversion Efficiency. *Nat. Commun.* **2013**, *4*, 1446.

(6) Xu, T.; Yu, L. How To Design Low Bandgap Polymers for Highly Efficient Organic Solar Cells. *Mater. Today* **2014**, *17*, 11–15.

(7) Boudreault, P.-L. T.; Najari, A.; Leclerc, M. Processable Low-Bandgap Polymers for Photovoltaic Applications. *Chem. Mater.* **2011**, *23*, 456–469.

(8) Chen, H.-C.; Chen, Y.-H.; Liu, C.-C.; Chien, Y.-C.; Chou, S.-W.; Chou, P.-T. Prominent Short-Circuit Currents of Fluorinated Quinoxaline-Based Copolymer Solar Cells with a Power Conversion Efficiency of 8.0%. *Chem. Mater.* **2012**, *24*, 4766–4772.

(9) Jung, J. W.; Jo, J. W.; Liu, F.; Russell, T. P.; Jo, W. H. A Low Band-Gap Polymer Based on Unsubstituted Benzo[1,2-*b*:4,5-*b*′]-dithiophene for High Performance Organic Photovoltaics. *Chem. Commun.* **2012**, *48*, 6933–6935.

(10) Jung, J. W.; Liu, F.; Russell, T. P.; Jo, W. H. Synthesis of Pyridine-Capped Diketopyrrolopyrrole and Its Use as a Building Block of Low Band-Gap Polymers for Efficient Polymer Solar Cells. *Chem. Commun.* **2013**, *49*, 8495–8497.

(11) Chen, J.-D.; Cui, C.; Li, Y.-Q.; Zhou, L.; Ou, Q.-D.; Li, C.; Li, Y.; Tang, J.-X. Single-Junction Polymer Solar Cells Exceeding 10% Power Conversion Efficiency. *Adv. Mater.* **2015**, *27*, 1035–1041.

(12) Liu, Y.; Zhao, J.; Li, Z.; Mu, C.; Ma, W.; Hu, H.; Jiang, K.; Lin, H.; Ade, H.; Yan, H. Aggregation and Morphology Control Enables Multiple Cases of High-Efficiency Polymer Solar Cells. *Nat. Commun.* **2014**, *5*, 5293.

(13) Liao, S.-H.; Jhuo, H.-J; Yeh, P.-N.; Cheng, Y.-S.; Li, Y.-L.; Lee, Y.-H.; Sharma, S.; Chen, S.-A. Single Junction Inverted Polymer Solar Cell Reaching Power Conversion Efficiency 10.31% by Employing Dual-Doped Zinc Oxide Nano-film as Cathode Interlayer. *Sci. Rep.* **2014**, *4*, 6813.

(14) Kaake, L. G.; Barbara, P. F.; Zhu, X.-Y. Intrinsic Charge Trapping in Organic and Polymeric Semiconductors: A Physical Chemistry Perspective. *J. Phys. Chem. Lett.* **2010**, *1*, 628–635.

(15) Zhu, X.; Fang, J.; Lu, K.; Zhang, J.; Zhu, L.; Zhao, Y.; Shuai, Z.; Wei, Z. Naphtho[1,2-*b*:5, 6-*b*′]dithiophene Based Two-Dimensional Conjugated Polymers for High Efficient Thick-Film Inverted Polymer Solar Cells. *Chem. Mater.* **2014**, *26*, 6947–6954.

(16) Zou, Y.; Najari, A.; Berrouard, P.; Beaupré, S.; Aich, B. R.; Tao, Y.; Leclerc, M. A Thieno[3,4-*c*]pyrrole-4,6-dione-Based Copolymer for Efficient Solar Cells. *J. Am. Chem. Soc.* **2010**, *132*, 5330–5331.

(17) Chu, T.-Y.; Lu, J.; Beaupre, S.; Zhang, Y.; Pouliot, J.-R.; Wakim, S.; Zhou, J.; Leclerc, M.; Li, Z.; Ding, J.; Tao, Y. Bulk Heterojunction Solar Cells Using Thieno[3,4-*c*]pyrrole-4,6-dione and Dithieno[3,2-*b*:2′,3′-*d*]silole Copolymer with a Power Conversion Efficiency of 7.3%. *J. Am. Chem. Soc.* **2011**, *133*, 4250–4253.

(18) Li, Z.; Tsang, S.-W.; Du, X.; Scoles, L.; Robertson, G.; Zhang, Y.; Toll, F.; Tao, Y.; Lu, J.; Ding, J. Alternating Copolymers of Cyclopenta[2,1-*b*;3,4-*b*′]dithiophene and Thieno[3,4-*c*]pyrrole-4,6-

DOI: 10.1021/acsami.5b03446
ACS Appl. Mater. Interfaces 2015, 7, 13666–13674

dione for High-Performance Polymer Solar Cells. *Adv. Funct. Mater.* **2011**, *21*, 3331−3336.
(19) Jo, J.; Pron, A.; Berrouard, P.; Leong, W. L.; Yuen, J. D.; Moon, J. S.; Leclerc, M.; Heeger, A. J. A New Terthiophene-Thienopyrrolodione Copolymer-Based Bulk Heterojunction Solar Cell with High Open-Circuit Voltage. *Adv. Energy Mater.* **2012**, *2*, 1397−1403.
(20) Yuan, J.; Zhai, Z.; Dong, H.; Li, J.; Jiang, Z.; Li, Y.; Ma, W. Efficient Polymer Solar Cells with a High Open Circuit Voltage of 1 V. *Adv. Funct. Mater.* **2013**, *23*, 885−892.
(21) Warnan, J.; Cabanetos, C.; Labban, A. E.; Hansen, M. R.; Tassone, C.; Toney, M. F.; Beaujuge, P. M. Ordering Effects in Benzo[1,2-*b*:4,5-*b*′]difuran Thieno[3,4-*c*]pyrrole-4,6-dione Polymers with >7% Solar Cell Efficiency. *Adv. Mater.* **2014**, *26*, 4357−4362.
(22) Kim, J.-H.; Park, J. B.; Xu, F.; Kim, D.; Kwak, J.; Grimsdale, A. C.; Hwang, D.-H. Effect of π-Conjugated Bridges of TPD-Based Medium Bandgap Conjugated Copolymers for Efficient Tandem Organic Photovoltaic Cells. *Energy Environ. Sci.* **2014**, *7*, 4118−4131.
(23) Chen, H.; Cuo, Y.; Yu, G.; Zhao, Y.; Zhang, J.; Gao, D.; Liu, H.; Liu, Y. Highly π-Extended Copolymers with Diketopyrrolopyrrole Moieties for High-Performance Field-Effect Transistors. *Adv. Mater.* **2012**, *24*, 4618−4622.
(24) Huang, H.; Chen, Z.; Ortiz, R. P.; Newman, C.; Usta, H.; Lou, S.; Youn, J.; Noh, Y.-Y.; Baeg, K.-J.; Chen, L. X.; Facchetti, A.; Marks, T. Combining Electron-Neutral Building Blocks with Intramolecular "Conformational Locks" Affords Stable, High-Mobility P- and N-Channel Polymer Semiconductors. *J. Am. Chem. Soc.* **2012**, *134*, 10966−10973.
(25) Kim, J. Y.; Qin, Y.; Stevens, D. M.; Ugurlu, O.; Kalihari, V.; Hillmyer, M. A.; Frisbie, C. D. Low Band Gap Poly(thienylenevinylene)/Fullerene Bulk Heterojunction Photovoltaic Cells. *J. Phys. Chem. C* **2009**, *113*, 10790−10797.
(26) Speros, J. C.; Paulsen, B. D.; White, S. P.; Wu, Y.; Jackson, E. A.; Slowinski, B. S.; Frisbie, C. D.; Hillmyer, M. A. An ADMET Route to Low-Band-Gap Poly(3-hexadecylthienylene vinylene): A Systematic Study of Molecular Weight on Photovoltaic Performance. *Macromolecules* **2012**, *45*, 2190−2199.
(27) Kim, J.; Lim, B.; Baeg, K.-J.; Noh, Y.-Y.; Khim, D.; Jeong, H.-G.; Yun, J.-M.; Kim, D.-Y. Highly Soluble Poly(thienylenevinylene) Derivatives with Charge-Carrier Mobility Exceeding 1 $cm^2 \cdot V^{-1} \cdot s^{-1}$. *Chem. Mater.* **2011**, *23*, 4663−4665.
(28) Cheon, Y. R.; Kim, Y. J.; Ha, J.-J.; Kim, M.-J.; Park, C. E.; Kim, Y.-H. TPD-Based Copolymers with Strong Interchain Aggregation and High Hole Mobility for Efficient Bulk Heterojunction Solar Cells. *Macromolecules* **2014**, *47*, 8570−8577.
(29) Jung, E. H.; Jo, W. H. π-Extended Low Bandgap Polymer Based on Isoindigo and Thienylvinylene for High Performance Polymer Solar Cells. *Energy Environ. Sci.* **2014**, *7*, 650−654.
(30) Jung, J. W.; Liu, F.; Russell, T. P.; Jo, W. H. A High Mobility Conjugated Polymer Based on Dithienothiophene and Diketopyrrolopyrrole for Organic Photovoltaics. *Energy Environ. Sci.* **2012**, *5*, 6857−6861.
(31) Jung, J. W.; Liu, F.; Russell, T. P.; Jo, W. H. Semi-crystalline Random Conjugated Copolymers with Panchromatic Absorption for Highly Efficient Polymer Solar Cells. *Energy Environ. Sci.* **2013**, *6*, 3301−3307.
(32) Wu, J.-L.; Chen, F.-C.; Hsiao, Y.-S.; Chien, F.-C.; Chen, P.; Kuo, C.-H.; Huang, M. H.; Hsu, C.-S. Surface Plasmonic Effects of Metallic Nanoparticles on the Performance of Polymer Bulk Heterojunction Solar Cells. *ACS Nano* **2011**, *5*, 959−967.
(33) Stuart, A. C.; Tumbleston, J. R.; Zhou, H. X.; Li, W. T.; Liu, S. B.; Ade, H.; You, W. Fluorine Substituents Reduce Charge Recombination and Drive Structure and Morphology Development in Polymer Solar Cells. *J. Am. Chem. Soc.* **2013**, *135*, 1806−1815.
(34) Cowan, S. R.; Wang, J.; Yi, J.; Lee, Y. J.; Olson, D. C.; Hsu, J. W. P. Intensity and Wavelength Dependence of Bimolecular Recombination in P3HT: PCBM Solar Cells: A White-Light Biased External Quantum Efficiency Study. *J. Appl. Phys.* **2013**, *113*, 154504.
(35) Liu, F.; Gu, Y.; Wang, C.; Zhao, W.; Chen, D.; Briseno, A. L.; Russell, T. P. Efficient Polymer Solar Cells Based on a Low Bandgap Semi-crystalline DPP Polymer-PCBM Blends. *Adv. Mater.* **2012**, *24*, 3947−3951.
(36) Lim, B.; Baeg, K.-J.; Jeong, H.-G.; Jo, J.; Kim, H.; Park, J.-W; Noh, Y.-Y.; Vak, D.; Park, J. H.; Park, J.-W.; Kim, D.-Y. A New Poly(thienylenevinylene) Derivative with High Mobility and Oxidative Stability for Organic Thin-Film Transistors and Solar Cells. *Adv. Mater.* **2009**, *21*, 2808−2814.
(37) Wang, D. H.; Pron, A.; Leclerc, M.; Heeger, A. J. Additive-Free Bulk-Heterojuction Solar Cells with Enhanced Power Conversion Efficiency, Comprising a Newly Designed Selenophene-Thienopyrrolodione Copolymer. *Adv. Funct. Mater.* **2013**, *23*, 1297−1304.
(38) Jung, J. W.; Jo, J. W.; Chueh, C.-C.; Liu, F.; Jo, W. H.; Russell, T. P.; Jen, A. K.-Y. Fluoro-Substituted n-Type Conjugated Polymers for Additive-Free All-Polymer Bulk Heterojunction Solar Cells with High Power Conversion Efficiency of 6.71%. *Adv. Mater.* **2015**, *27*, 3310−3317.
(39) Jung, J. W.; Liu, F.; Russell, T. P.; Jo, W. H. Anthracene-Based Medium Bandgap Conjugated Polymers for High Performance Polymer Solar Cells Exceeding 8% PCE without Additive and Annealing Process. *Adv. Energy Mater.* **2015**, *5*, 1500065.
(40) Jung, J. W.; Jo, W. H. Low Band-Gap Copolymer Composed of Thienyl Substituted Anthracene and Diketopyrrolopyrrole Compatible with Multiple Electron Acceptors for High Efficiency Polymer Solar Cells. *Polym. Chem.* **2015**, *6*, 4013−4019.

DOI: 10.1021/acsami.5b03446
ACS Appl. Mater. Interfaces 2015, 7, 13666−13674